# Attenuation of acoustic waves in glacial ice and salt domes

P. B. Price

Physics Department, University of California, Berkeley, California, USA

Received 24 June 2005; revised 20 September 2005; accepted 4 November 2005; published 8 February 2006.

[1] Two classes of natural solid media, glacial ice and salt domes, are under consideration as media in which to deploy instruments for detection of neutrinos with energy $\geq 10^{18}$ eV. Though insensitive to $10^{11}$ to $10^{16}$ eV neutrinos for which observatories (e.g., AMANDA and IceCube) that utilize optical Cherenkov radiation detectors are designed, radio and acoustic methods are suited for searches for the very low fluxes of neutrinos with energies $>10^{17}$ eV. This is because owing to the very long attenuation lengths of radio and acoustic waves produced by interactions of such neutrinos in ice and salt, detection modules can be spaced at horizontal distances $\sim$1 km, in contrast to the 0.12 km distances between strings of IceCube modules. In this paper, I calculate the absorption and scattering coefficients as a function of frequency and grain size for acoustic waves in glacial ice and salt domes and show that experimental measurements on laboratory samples and in glacial ice and salt domes are consistent with theory. For South Pole ice with grain size $\sim$0.2 cm at depths $\leq$600 m, scattering lengths are calculated to be 2000 and 25 km at frequencies 10 and 30 kHz, respectively; for grain size $\sim$0.4 cm at 1500 m (the maximum depth to be instrumented acoustically), scattering lengths are calculated to be 250 and 3 km. These are within the range of frequencies where most of the energy of the acoustic wave is concentrated. The absorption length is calculated to be $9 \pm 3$ km at all frequencies above $\sim$100 Hz. For NaCl (rock salt) with grain size 0.75 cm, scattering lengths are calculated to be 120 and 1.4 km at 10 and 30 kHz, and absorption lengths are calculated to be $3 \times 10^4$ and 3300 km at 10 and 30 kHz. Existing measurements are consistent with theory. For ice, absorption is the limiting factor; for salt, scattering is the limiting factor. Both media would be suitable for detection of acoustic waves from ultrahigh-energy neutrino interactions.

**Citation:** Price, P. B. (2006), Attenuation of acoustic waves in glacial ice and salt domes, *J. Geophys. Res.*, *111*, B02201, doi:10.1029/2005JB003903.

## 1. Introduction

[2] IceCube, the first kilometer-scale neutrino observatory, is now under construction in South Pole ice. It will have 80 strings, each instrumented with 60 phototubes at depths from 1450 to 2450 m in a 1 km $\times$ 1 km $\times$ 1 km volume [*Ahrens et al.*, 2004]. The timing and strength of flashes of optical Cherenkov radiation recorded in the phototubes enable the direction and energy of an interacting neutrino to be reconstructed. Because the neutrino flux falls off so rapidly with energy, an observatory far larger than 1 km$^3$ will be required in order to detect neutrinos with energies above $\sim 10^{18}$ eV. Those ultrahigh energy neutrinos are predicted to have great cosmological significance and may reveal new physics beyond the standard model. The Greisen-Zatsepin-Kuzmin (GZK) neutrinos, with energies $\sim 10^{17}$–$10^{20}$ eV, which should result from interactions of high-energy cosmic ray protons with the 2.7°K cosmic background photons, are an example. Estimates indicate that no more than $\sim$1 GZK neutrino per year can be detected with IceCube. With a future observatory of effective volume more than an order of magnitude larger than IceCube, it may be possible to probe new physics and predictions of some cosmological models. Simulations of detection rates of such neutrinos have led to a straw design of a hybrid optical/radio/acoustical neutrino detector with $>10^2$ km$^3$ effective volume [*Besson et al.*, 2005]. At its core would be the IceCube optical array. A combination of radio receivers and acoustic transducers would extend outward from IceCube with lateral extent at least 10 km x 10 km, would be instrumented from depths of $\sim$5 to $\sim$1500 m, and would thus be situated essentially entirely in ice at shallower depths than IceCube. They could be sparsely spaced because the attenuation lengths of radio and acoustic waves from ultrahigh-energy neutrino interactions are expected to be much greater than for visible light. The occasional detection of an ultrahigh-energy neutrino with optical modules in coincidence with radio and acoustical modules would validate the radio and acoustical techniques, which are insensitive to neutrino interactions except at energies above $\sim 10^{17}$ eV.

[3] With the idea of a future gigantic neutrino observatory in mind, some years ago I discussed the absorption and


0148-0227/06/2005JB003903$09.00

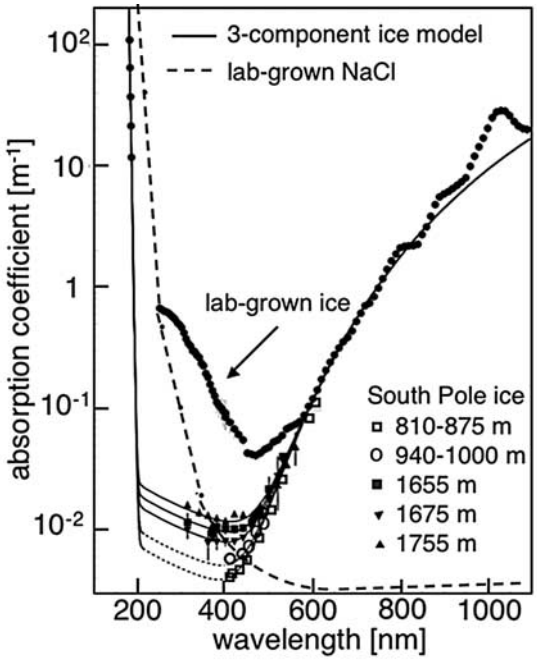


**Figure 1.** Absorptivity of laboratory ice, of South Pole ice (K. Woschnagg et al., Optical properties of deep glacial ice at the South Pole, submitted to *Applied Optics*, 2005), and of NaCl [*Palik*, 1985]. South Pole ice is optimally transparent for Cherenkov light; NaCl is transparent at wavelengths from ~0.5 to 5 μm, in the tail of the Cherenkov distribution. The theory for the three-component ice model is given by *AMANDA Collaboration* [1997].

scattering of acoustic waves in the 2.8-km-deep glacial ice at the South Pole [*Price*, 1993]. Since then, a number of workers have been investigating the feasibility of detecting ultrahigh-energy neutrino interactions in underground NaCl domes, of typical dimensions ~3 km × ~4 km × ~5 km, using either radio or acoustic receivers. In support of those efforts, in this paper I discuss theory and measurements of acoustic attenuation in laboratory samples and in situ in natural media for both ice and salt. I consider only longitudinal (pressure) waves, since the efficiency for production of transverse (shear) waves associated with an electromagnetic cascade is low and uncertain.

## 2. Absorptivity of Optical Cherenkov Radiation at 200–2000 nm in Ice and Salt

[4] Before discussing acoustic propagation, a brief remark on propagation of optical Cherenkov radiation is in order. High-purity Antarctic ice [*Askebjer et al.*, 1997] and high-purity NaCl [*Palik*, 1985] happen to be the two most optically transparent solids known. Figure 1 compares laboratory-grown ice, ice at various depths at the South Pole, and laboratory-grown salt in the UV, visible, and IR. Despite the extremely small absorption coefficient of NaCl at wavelengths longer than ~500 nm, more light from Cherenkov radiation by a neutrino-induced cascade or muon would be detected in a phototube immersed in Antarctic ice than in a salt dome. This disadvantage of salt relative to ice is due to the rapid decrease of Cherenkov light intensity with wavelength, $\lambda$: $(dI/d\lambda)_{\text{Cherenkov}} \propto \lambda^{-2}$. Ice is far more transparent than salt to light at $\lambda < 400$ nm, where the Cherenkov light intensity is most intense. The abrupt increase in absorptivity at $\lambda < 200$ nm is a consequence of photon energy exceeding the band gap and being able to eject electrons. The drawback to using visible light to detect ultrahigh-energy neutrino interactions in either ice or salt is that absorption lengths are typically only $\sim 10^2$ m. This limits the size of an observatory on the grounds of cost, since the detection and reconstruction of events requires that the spacing of phototubes be $\leq$ absorption length. To fill $10^2$ km$^3$ of ice or salt with phototubes would thus be prohibitively expensive.

## 3. Conversion of Ionization Energy Into Acoustic Energy

[5] The conversion of ionization energy in a neutrino-induced electromagnetic cascade of electrons, positrons, and gamma rays into acoustic energy is orders of magnitude less efficient than its conversion into visible light. The thermoacoustic model [*Askariyan*, 1979] is based on the fact that in a condensed medium, the energy in an electromagnetic cascade resulting from the neutrino interaction is concentrated in a roughly cylindrical volume of length $L \approx 5$ m and diameter ~5 cm in a liquid or solid. The resulting almost instantaneous deposition of ionization energy raises the volume of the cylindrical region to a high temperature, leading to a bipolar pressure pulse that is mostly in directions orthogonal to the axis of the cylinder. The amplitude of the pulse is a measure of the cascade energy. In the near field (distances $\ll L^2/\lambda$), the pulse propagates radially from the axis of the cylinder like a radially expanding flat disk, providing information on the direction of the incoming cascade. Only in the far field (at a distance $\gg L^2/\lambda$ of order kilometers) does the wave front assume a roughly spherical shape. The frequency of the pressure wave is in the 10 to 60 kHz range and is related to the transverse dimension of the cascade. Table 1 compares the figures of merit for seawater, ice, and NaCl as media for conversion of ionization energy in a cascade into the energy in the resulting pressure wave. Reading downward in the left-hand column, the parameters in Table 1 are temperature ($T$), longitudinal sound speed ($\nu_L$), volume coefficient of thermal expansion ($\beta$), specific heat at constant pressure ($C_p$), frequency at which the energy in the expanding wave is a maximum ($f_{\max}$), and Grüneisen parameter ($\gamma$). The latter, which appears in the solution to the thermoelastic equation for sound generation, is a dimensionless parameter proportional to the wave amplitude at fixed distance from the cylinder [*Lyamshev*, 1992]. The values of the Grüneisen parameter show that ice is a factor 7.3 more effective than

**Table 1.** Conversion of Ionization Energy Into Acoustic Energy

| Parameter | Ocean | Ice | NaCl |
|---|---|---|---|
| $T$, °C | 15 | −51 | 30 |
| $\langle \nu_L \rangle$, m s$^{-1}$ | 1530 | 3920 | 4560 |
| $\beta$, m$^3$ m$^{-3}$ K$^{-1}$ | $25.5 \times 10^{-5}$ | $12.5 \times 10^{-5}$ | $11.6 \times 10^{-5}$ |
| $C_p$, J kg$^{-1}$ K$^{-1}$ | 3900 | 1720 | 839 |
| $f_{\max}$, kHz | 7.7 | 20 | 42 |
| Grüneisen parameter $\gamma \equiv \langle \nu_L \rangle^2 \beta / C_p$ | 0.153 | 1.12 | 2.87 |

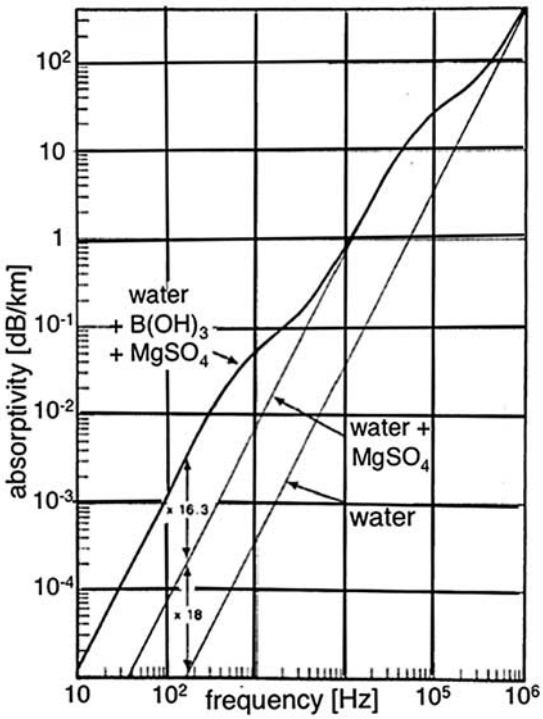


**Figure 2.** Acoustic absorptivity in seawater at 4°C and 1 atmosphere (adapted from *Fisher and Simmons* [1977]).

seawater (and a factor 10 more effective than lake water), and NaCl is a factor 2.6 more effective than ice.

[6] In addition to conversion efficiency, ambient noise is also an important consideration. The noise level in the ocean, due to wind, waves, and organisms, is far higher than in glacial ice or in a salt dome and disfavors ocean as a medium for an acoustic array. See section 9.

## 4. Refraction and Absorptivity of Acoustic Waves in the Ocean

[7] Scattering of acoustic waves in the ocean is negligible. Refraction depends on the gradient of acoustic velocity, which is a function of both temperature and density. To a good approximation, the refractive index and sound speed vary only in the vertical ($z$) direction. This leads to two equations, valid provided the refractive index does not change much over the distance of one wavelength. The first, Snell's law for refraction of an acoustic wave, relates the angle $\theta$ of a particular ray to the horizontal to the initial angle $\theta_0$ when at a depth where the refractive index is $n$:

$$\frac{\cos\theta}{\cos\theta_0} = \frac{v}{v_0} \equiv \frac{1}{n} \tag{1}$$

The second states that the curvature of a ray, $d\theta/ds$, is directly proportional to the velocity gradient:

$$\frac{d\theta}{ds} = -K\frac{dv}{dz} = -\frac{\cos\theta_0}{v_0}\frac{dv}{dz} = \frac{1}{R} \tag{2}$$

where $R$ is the radius of curvature. For a constant velocity gradient, the curvature along any given ray is constant, so the ray is the arc of a circle. Curvature distorts the expanding disc-shaped acoustic wave, requiring that its amplitude and arrival time at each of a number of acoustic sensors be recorded in order to reconstruct the location and orientation of the original cascade.

[8] Figure 2 shows the frequency-dependent contributions to absorptivity in seawater at 4°C and 1 atm. Absorptivity also depends weakly on depth (and hence on pressure). At frequencies above ~500 kHz, it behaves in the same manner as fresh water, with energy dissipation resulting from viscosity of the water. At lower frequencies, pressure-dependent chemical reactions can cause acoustic absorption. Pressure waves shift chemical equilibria between dissolved molecular compounds and their dissociated ions, taking energy from the waves. For frequencies up to nearly 10 kHz, absorption is caused primarily by the presence of boric acid, whose dissociation has a time constant such that energy-absorbing shifts in its equilibrium cannot take place in times shorter than a few tenths of a millisecond. At higher frequencies, up to a few hundred kHz, a dissociation process associated with dissolved $MgSO_4$ produces the energy losses. The equations for $B(OH)_3$ and $MgSO_4$ are

$$B(OH)_3 = B^{3+} + 3\ OH^- \tag{3}$$

(relaxation frequency ~1 kHz) and

$$MgSO_4 = Mg^{2+} + SO_4^{2-} \tag{4}$$

(relaxation frequency ~100 kHz). Absorptivities of other salts in seawater are negligible by comparison.

## 5. Acoustic Refraction and Scattering in Ice

### 5.1. Refraction in Firn Ice

[9] Refraction of acoustic waves in firn ice is qualitatively similar to that in lunar soil in that both curve upward due to the monotonic increase of density and thus of acoustic speed with depth. Seismologists found that low-frequency propagation of seismic waves from meteorite impacts on the lunar surface propagated completely around the moon due to the waveguide effect of the density gradient in the lunar soil [*Gold and Soter*, 1970].

[10] If the velocity as a function of depth in firn has been measured, equations (1) and (2) can be used to derive the ray paths. *Albert* [1998] has used the equations, together with wave number integration, to model seismic noise propagation at 3, 10, and 30 Hz as a function of firn depth and horizontal distance from the South Pole station. At those low frequencies he found that the reduction in wave amplitude with depth and distance is due mainly to wave front spreading and to upward curvature in the firn, not to absorption or scattering. However, at frequencies relevant to detection of neutrino-induced cascades, we have neither experiment nor theory to guide in modeling attenuation until a depth below pore closeoff is reached. From there downward, the discussions in sections 5.2 and 5.3 on scattering and in section 6 on absorption apply.

### 5.2. Scattering in Bubbly Ice

[11] The mean diameter of air bubbles decreases monotonically with depth from the bottom of the firn layer, at

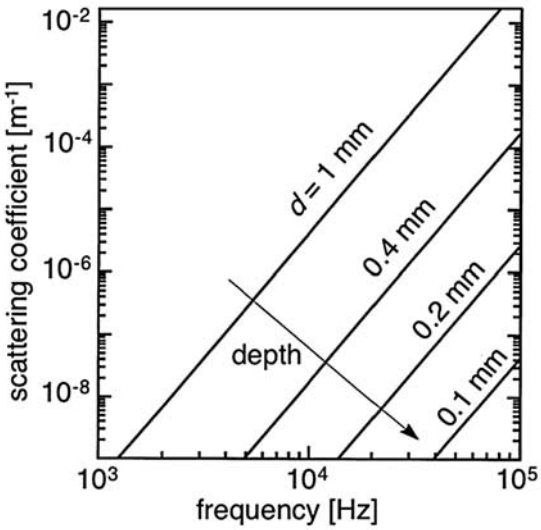


**Figure 3.** Calculated scattering from air bubbles with diameter ranging from 1 mm near the surface to 0.1 mm at a depth of 1000 m in South Pole ice (reprinted with permission from *Price* [1993], Acoustical Society of America). Bubble density is 200 $cm^{-3}$.

~100 m, to ~1400 m, below which all bubbles have converted into the solid clathrate phase. The density of clathrate crystals is close to that of ice, so the scattering of acoustic waves by clathrates is negligibly small. In the bubbly regime, the mean spacing between bubbles is much greater than their linear dimensions, and they act as independent scatterers. For frequencies of interest here, the Rayleigh approximation ($\lambda/2\pi d_b > 1$, where $d_b$ is bubble diameter) is valid. As shown in Figure 3, the scattering coefficient for a longitudinal wave depends on bubble concentration, $n_0$, as well as on $d_b$ and frequency, $f$ [*Price*, 1993].

$$b_{\text{bubble}}\left[m^{-1}\right] = 2.68 \times 10^{-10}\left(n_o/200\ \text{cm}^{-3}\right) \cdot (d_b/0.02\ \text{cm})^6 (f/10\ \text{kHz})^4 \quad (5)$$

Equation (5) is written in such a way as to simplify scaling from canonical values $n_o$ = 200 $cm^{-3}$, $d_b$ = 0.02 cm, $f$ = 10 kHz, and $b_{\text{bubble}} = 2.68 \times 10^{-10}$ m to any other values. At all depths below the firn, scattering from bubbles is weaker than from grain boundaries, which will be discussed in section 5.3.

### 5.3. Scattering at Grain Boundaries

[12] In an elastically isotropic solid such as glass, the speed of elastic waves is independent of direction, and there is no scattering. In crystalline solids, scattering occurs at grain boundaries, due to abrupt changes in the acoustic speed. At all depths in terrestrial glacial ice the crystal structure is hexagonal, and the acoustic properties are functions of the five elastic constants $c_{11}$, $c_{12}$, $c_{13}$, $c_{33}$, and $c_{44}$. There are three distinct scattering regimes, depending on the magnitude of the parameter $\lambda/2\pi d$, where $d$ is the mean diameter of the grain in polycrystalline ice. In the Rayleigh regime ($\lambda/2\pi d > 1$), the scattering coefficient $b(d, f)$ is proportional to $d^3 f^4$. For longitudinal and transverse waves in a solid with randomly oriented crystals with hexagonal structure, *Merkulov* [1957a] derived

$$b_L = \frac{2\pi^4 d^3 f^4}{1350\rho^2 v_L^3}\left(\frac{a_1}{v_L^5} + \frac{b_1}{v_T^5}\right) \qquad b_T = \frac{2\pi^4 d^3 f^4}{1350\rho^2 v_T^3}\left(\frac{a_2}{v_L^5} + \frac{b_2}{v_T^5}\right) \quad (6)$$

where $\rho$ is density, $v_L$ and $v_T$ are longitudinal and transverse wave speeds, and the dependences of the coefficients $a_1$, $b_1$, $a_2$, and $b_2$ on the elastic constants of ice are given by *Price* [1993]. The two terms in parentheses take into account conversion between the two modes during scattering at grain boundaries. In South Pole ice with $v_L$ = 3920 m $s^{-1}$ and $v_T$ = 1995 m $s^{-1}$, in the Rayleigh regime,

$$b_L = 5 \times 10^4 (d/0.2\ \text{cm})^3 (f/10\ \text{kHz})^4 \left[\text{km}^{-1}\right] \quad (7)$$

In the stochastic regime ($0.5 < \lambda/2\pi d < 1$), the scattering deviates from the Rayleigh law, increasing only as $df^2$ [*Merkulov*, 1957a]. The result for ice is

$$b_L = 6.2(d/0.2\ \text{cm})(f/500\ \text{kHz})^2 \left[\text{m}^{-1}\right] \quad (8)$$

This weaker dependence on $d$ and $f$ is caused by the coherent nature of the scattering process. For $d$ = 0.2 cm, equation (8) holds in the frequency regime 310 kHz < $f$ < 620 kHz.

[13] In the geometric regime ($\lambda/2\pi d < 0.5$), the quadratic dependence of $b_T$ on frequency disappears, and the scattering mechanism approaches a diffusive process [*Merkulov*, 1957b]. The wave velocity shows a discontinuity in magnitude and direction at each grain boundary, and some of the energy is reflected at the boundary. The resulting scattering is independent of frequency and inversely proportional to mean grain diameter:

$$b_L = \langle R \rangle / d \quad (9)$$

For the case of ice, for which the elastic anisotropy of individual crystal grains is small, the average reflection coefficient is given by $\langle R \rangle$ = 0.068 (see *Price* [1993] for details), and

$$b_L\left[\text{m}^{-1}\right] = 6.8/d[\text{cm}] \quad (10)$$

For $d$ = 0.2 cm, this leads to $b_L \approx 34\ \text{m}^{-1}$, valid at frequencies above ~620 kHz. Note that the energy is not lost, merely redirected. For all cases of interest ($d$ < 1 cm), the frequency at which scattering reaches its limiting value is above 100 kHz.

[14] Figure 4 shows the dependence of grain boundary scattering on grain diameter and frequency for frequencies relevant to neutrino-induced hydrodynamic wave propagation and for a random distribution of c axes. In the top 600 m, the grain diameter is no larger than ~0.2 cm, below which it slowly increases with depth. Although no ice core deeper than ~300 m in South Pole ice has been taken, one can estimate grain size at greater depths in South Pole ice by interpolating between measured values for Vostok Station, Antarctica, with lower temperature and snow accumulation rate, and values for the Greenland Ice Sheet Project (GRIP) site, with higher temperature and accumulation rate [*De La*

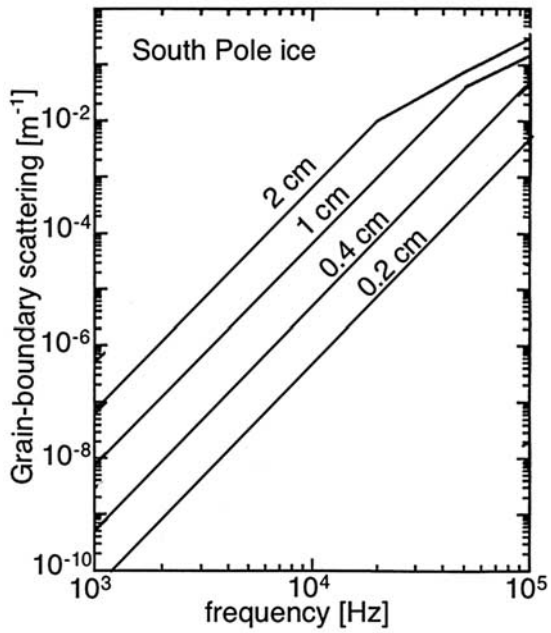


**Figure 4.** Scattering as function of frequency and grain diameter in South Pole ice at any temperature [*Price*, 1993].

*Chapelle et al.*, 1998]. In both cases the grain size grows only to ~0.4 cm at 1500 m, the maximum depth envisaged for an acoustic array. One sees from Figure 4 that acoustic scattering in ice with 0.2 to 0.4 cm grain diameter is quite low: in the frequency regime where the acoustic energy of a neutrino-induced cascade is concentrated, the scattering length, defined as $1/b_L$, is 2000 km at 10 kHz, 25 km at 30 kHz, and 2 km at 60 kHz for depths $\leq$600 m, and gradually decreasing to 1/8 of those values at the greatest depth where an acoustic array is envisaged (1500 m). Thus, at all depths where an acoustic neutrino array will be located, scattering lengths are much larger than the optical values for IceCube, and the scattering coefficient is extremely small.

[15] When texture is taken into account, the magnitude of the scattering coefficient will be even smaller than in Figure 4. The acoustic velocity depends only on the angle of the propagation vector with respect to the c axis: for example, it is ~7% greater along the c axis than at an angle of 50° and ~3.5% greater than at 90° [see *Price*, 1993, Figure 2]. With increasing depth, the c axes become strongly aligned along the vertical direction in GRIP ice [*Thorsteinsson et al.*, 1997] and in a girdle pattern [*Lipenkov et al.*, 1989] in Vostok ice. In the limit of perfect alignment of c axes, there would be no grain boundary scattering; for c axes aligned to within 15° of vertical, grain boundary scattering would be reduced by a factor 10 [*Price*, 1993]. Thus the estimates in Figure 4 are upper limits, since they neglect anisotropic texture.

## 6. Acoustic Absorption in Ice

[16] For longitudinal waves in very cold South Pole ice, where the temperature is −51°C near the surface and rises slowly to −46°C at 1000 m, the dominant relaxation mechanism is proton reorientation, whereas in warm ice near bedrock, where the temperature is no lower than −9°C [*Price et al.*, 2002], grain boundary sliding would dominate. We consider only proton reorientation [*Paterson*, 1994], which dominates in South Pole ice at depths less than ~2000 m where the acoustic ultrahigh-energy neutrino astrophysics observatory mentioned in section 1 is under consideration for development after the completion of IceCube [*Besson et al.*, 2005]. The contribution of proton reorientation to absorption is independent of grain size and texture, whereas the contribution of grain boundary sliding to absorption in warm ice would depend on both. The dipole moment of the $H_2O$ molecule may assume one of six orientations. Passage of an elastic wave may result in movement of some of the protons, causing rotation of dipole moments into favored orientations. The rotation proceeds by the movement of orientational defects, whose concentration increases with temperature, from one hydrogen bond to another. As Figure 5 (top) shows, D and L defects denote bond sites occupied by two protons (D for the German word "doppel" or double) and no protons (L for "leer" or empty). In addition, ionization defects, $OH^-$ (only 1 proton attached to an oxygen) and $H_3O^+$ (3 protons attached to an oxygen) can migrate via a shift of a proton along the same hydrogen bond from one oxygen to another in response to an acoustic wave. Defect reorientation and migration lead to

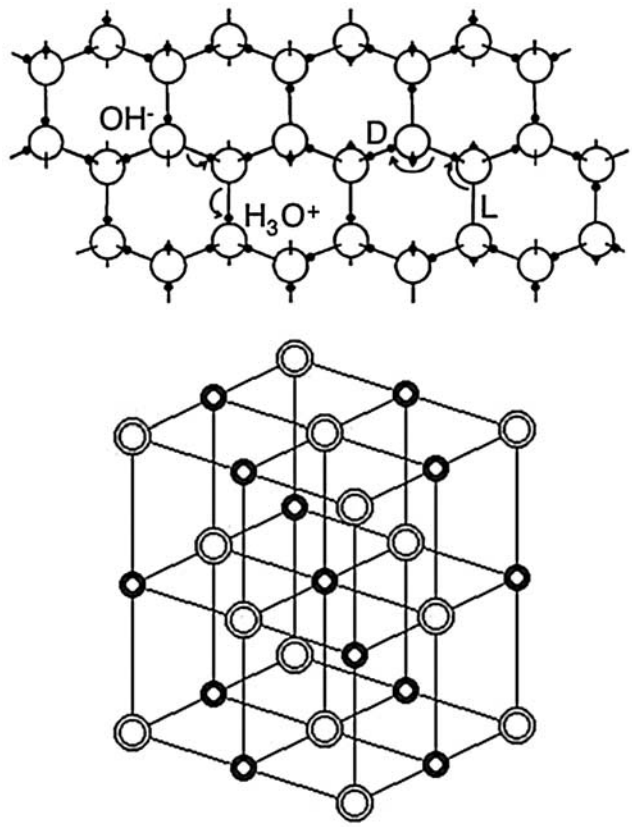


**Figure 5.** Structures of ice and NaCl: (top) View of a plane through ice; an acoustic wave moves protons from one bond site to another by motion of four kinds of defects. (bottom) In NaCl, there are no protons; instead, acoustic phonons (quantized lattice vibrations) extract energy by colliding inelastically with the Planck distribution of thermal phonons.

**Table 2.** Measured Parameters for Calculations of Absorptivity of Ice Versus Frequency and Temperature

| Reference | Structure | Frequencies, Hz | $U$, eV | $\tau_o$, s | Average $\delta_{max}$ | $\lambda_a$, km | |
|---|---|---|---|---|---|---|---|
| | | | | | | $-51°$, $f > 100$ Hz | $-46°$, $f > 100$ Hz |
| *Schiller* [1958] | monocrystal,two angles | 800–6000 | 0.58 | $3 \times 10^{-16}$ | 0.0094 | 5.7 | 2.9 |
| *Kuroiwa* [1964] | polycrystal | 177–790 | 0.57 | $6.9 \times 10^{-16}$ | 0.0087 | 8.6 | 4.5 |
| *Oguro et al.* [1982] | monocrystal, eight angles | 400 and 2000 | 0.60 | $1.7 \times 10^{-16}$ | 0.0074 | 11.7 | 5.9 |

"internal friction", with a relaxation time $\tau_m(T) = \tau_o \exp(U/kT)$, where $U$ is the activation energy for mechanical relaxation. The logarithmic decrement for energy loss due to the acoustic wave is given by [*Fletcher*, 1970]

$$\delta = \delta_{max} \frac{4\pi f \tau_m}{1 + 4\pi^2 f^2 \tau_m^2} \tag{11}$$

where $\delta_{max}$ is a constant, independent of frequency, with a value that depends on the wave mode and the direction of propagation. For polycrystalline ice with randomly oriented grains, an experimentally determined average value can be taken. Because of the low temperature in the top ~600 m of South Pole ice, there is essentially no shear at those depths, which validates the assumption of randomly oriented grains and of an average value of $\delta_{max}$. The absorptivity and absorption length are then given by

$$a_L\left[\mathrm{m}^{-1}\right] \equiv 1/\lambda_a = \delta f / v_L \tag{12}$$

where $\delta$ has a temperature dependence contained in $\tau_m(T)$.

[17] Table 2 summarizes the results of three sets of measurements of $U$, $\tau_o$, and $\delta_{max}$ obtained from internal friction measurements of laboratory ice samples. The last two columns give the values of absorption length at near-surface temperature ($-51°$C) and at 1000 m ($-46°$C) in South Pole ice, calculated from the measurements of $U$, $\tau_o$, and $\delta_{max}$.

[18] Figure 6 shows curves of absorptivity as a function of frequency at several temperatures, calculated from data of *Kuroiwa* [1964]. As Table 2 shows, his values of absorption length fall between those generated from the data of *Schiller* [1958] and of *Oguro et al.* [1982]. In addition, several field measurements have been reported. *Bentley and Kohnen* [1976] measured seismic attenuation of longitudinal waves in ice at depths 100 to 500 m and a temperature $-28°$C near Byrd Station at 136 Hz (solid circle in Figure 6), and they used reflection shooting in Antarctica and Greenland to infer internal friction at 50 to 200 Hz. Their results were similar to those obtained by *Brockamp and Kohnen* [1965] at $-22°$C in Greenland ice (solid triangle). Both points agree well with the calculations for the respective temperatures.

[19] One could make a case for adopting the data of *Oguro et al.* [1982] on the ground that they were obtained some 18 years after *Kuroiwa's* [1964] data. To be conservative, I use Kuroiwa's data and take the spread among the three authors as an indication that the uncertainty is ~±30%.

## 7. Scattering of Acoustic Waves in NaCl

[20] *Gorham et al.* [2002] have discussed the suitability of large rock salt formations for detection of ultrahigh-energy neutrinos, and *Jackson et al.* [1994] have discussed their structural dynamics. Salt evaporite beds such as are used as repositories for nuclear waste have NaCl layers >100 m thick separated by other minerals. Impurity contents include >1% water, mostly in liquid inclusions, as well as horizontal thin beds of clay, silt, and anhydrite ($CaSO_4$), and nuggets of sulfur, calcite, and $BaSO_4$ – all of which make evaporite beds unattractive for acoustic detection of neutrino cascades. Salt domes are purer than evaporite beds and probably have much longer absorption lengths. Several mines are known to consist of >99% polycrystalline NaCl and contain only 2 to 40 ppm water. The salt grains dynamically recrystallize while the dome is plastically deforming due to its lower density than that of surrounding rock. Scattering occurs at boundaries of recrystallized grains. Table 3 lists average grain sizes for a number of salt domes. Boundaries of subgrains inside grains have misorientations <1° where scattering is negligible. Scattering can also occur at interfaces between NaCl and layers of clay or anhydrite.

[21] As Figure 5 (bottom) shows, the crystal structure of NaCl is cubic, and the elastic properties depend on only three elastic constants, $c_{11}$, $c_{12}$, and $c_{44}$. The equations for grain boundary scattering for a crystal with cubic structure are slightly different from those for the hexagonal structure

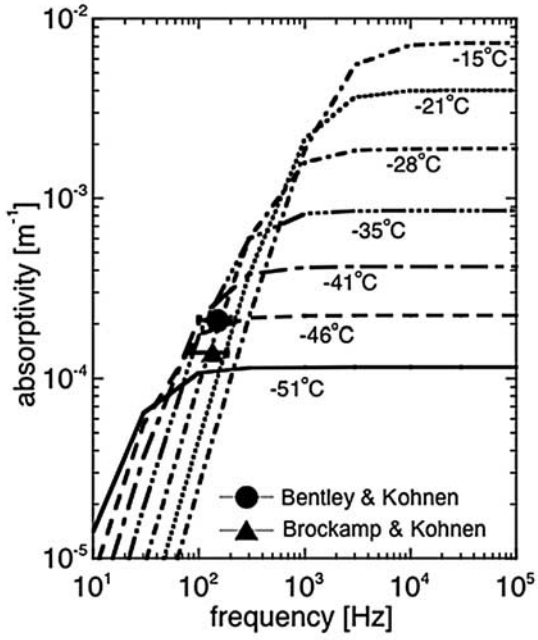


**Figure 6.** Temperature- and frequency-dependent absorptivity in polycrystalline ice calculated from laboratory measurements of internal friction by *Kuroiwa* [1964]. See text for discussion of in situ data in glacial ice (solid triangle and solid circle).

**Table 3.** Grain Sizes of NaCl in Salt Domes

| Location | Mean Grain Size in Samples Examined |
|---|---|
| Avery Island, Louisiana | ~7.5 mm |
| Bryan Mound, Texas | 2 to 40 mm; average 8 mm |
| Big Hill, Texas | 3.7 to 60 mm |
| West Hackberry, Louisiana | 6 to 30 mm |
| Moss Bluff, Texas | average 11 mm |
| Bayou Choctaw, Louisiana | 10 to 20 mm (at 0 to 728 m) |
| Zuidwending, Netherlands | 25% have $d$ = 1–3 mm; 75% have $d$ = 3–10 mm |
| Hockley Mine, Texas | 6–8 mm (with 0.1–1 mm anhydrite layers at grain boundaries) |

[*Merkulov*, 1957a, 1957b]. Equations (13) and (14) apply in the Rayleigh and stochastic regime, respectively:

$$b_L(\text{Rayleigh}) = \frac{4\pi^4 d^3 f^4}{1125}\,\frac{(c_{11}-c_{12}-2c_{44})^2}{\rho^2 v_L^3}\left[\frac{2}{v_L^5}+\frac{3}{v_T^5}\right] = 2\times 10^{-5}\left(\frac{d}{1\text{cm}}\right)^3\left(\frac{f}{10^4}\right)^4 m^{-1} \quad (13)$$

$$b_L(\text{stochastic}) = \frac{16\pi^2 d f^2}{525}\,\frac{(c_{11}-c_{12}-2c_{44})^2}{\rho^2 v_L^6} = 3.6\times 10^{-4}\left(\frac{d}{1\text{cm}}\right)\left(\frac{f}{10^4}\right)^2 m^{-1} \quad (14)$$

The values of $c_{ij}$ are given by *Merkulov et al.* [1970].

[22] Figure 7 gives my calculated values of scattering coefficient in polycrystalline NaCl as a function of frequency for mean grain diameters 0.2 to 2 cm. The points labeled with triangles show my analyses of acoustic amplitudes at frequencies 20 to 100 kHz at distances 7 and 71 m from a transmitter at a depth of 500 m in a salt repository in Morsleben, Germany [*Manthei and Eisenblätter*, 2005]. Although grain size was not measured, I infer from the similarity of the scattering coefficients to the dashed curve that the mean grain diameter was ~1 cm. Points labeled with solid deltas in Figure 7 were measured at 58 to 64 kHz at a depth of 470 m in the Hockley Salt Mine, Texas [*Kirby*, 2004]. The scattering coefficient is a factor ~10 higher than would be expected for the measured mean grain size of 0.6 to 0.8 cm. M. Fink (private communication, 2005) pointed out that a 0.1- to 1-mm-thick layer of powdery anhydrite is present in the grain boundaries. In my opinion, this could provide enough additional scattering to account for the high values of attenuation in the Hockley Mine. One should choose a salt dome where there is no anhydrite layer in the grain boundaries.

## 8. Absorption of Acoustic Waves in NaCl

[23] The absorptive mechanism that dominates in ice does not apply in NaCl, because the structure of NaCl has no protons and no hydrogen bonds. Experimental studies have shown that a potentially important relaxation mechanism, in which dislocations are driven by an acoustic wave, can also be neglected if the NaCl crystals have been well annealed. In salt repositories, the strain rate is so slow that ongoing annealing at ambient temperature maintains a fairly low dislocation density. The dominant absorption mechanism is due to phonon-phonon interactions, which were first discussed by *Akhieser* [1939] and quantitatively evaluated by *Merkulov et al.* [1970], *Sahasrabudhe and Lambade* [1998], and others. In this process, through anharmonic interactions, the entire thermal phonon gas extracts energy from the phonons that compose the acoustic wave. Sahasrabudhe and Lambade compared their calculations with data for NaCl, NaF, and LiF in three crystallographic directions at temperatures from 80 K to 300 K. They found no significant dependence of attenuation on temperature in the range studied, and their calculated values agreed with measured values to within ~10%. The absorptivity due to the Akhieser relaxation mechanism is

$$a_L[m^{-1}] = \frac{E_0 D}{6\rho v_L^3}\,\frac{4\pi^2 f^2 \tau_L}{(1+4\pi^2\tau_L^2)} \quad (15)$$

where $E_0$ is the thermal energy density, $\rho$ is the density, $v_L$ is the longitudinal wave velocity, and $D$ is the nonlinearity constant, which is derived from the second- and third-order elastic constants. The relaxation time $\tau_L$ for exchange of acoustic and thermal energies is given by $\tau_L = 3K/C_v\langle V\rangle^2$, where $K$ is the thermal conductivity (carried entirely by phonons if the crystal is nonconducting), $C_v$ is the specific heat per unit volume, and $\langle V\rangle$ is the average Debye velocity. For details, see *Kor and Mishra* [1975].

[24] For $2\pi f\tau_L \ll 1$, the relaxation equation for absorptivity (15) simplifies to

$$a_L = 2E_0 D\pi^2 f^2 \tau/3\rho v_L^3 \quad (16)$$

Using the values of $K$, $C_v$, and $\langle V\rangle^2$ for NaCl [*Merkulov et al.*, 1970] leads to a relaxation time of $\sim 10^{-11}$ s, from

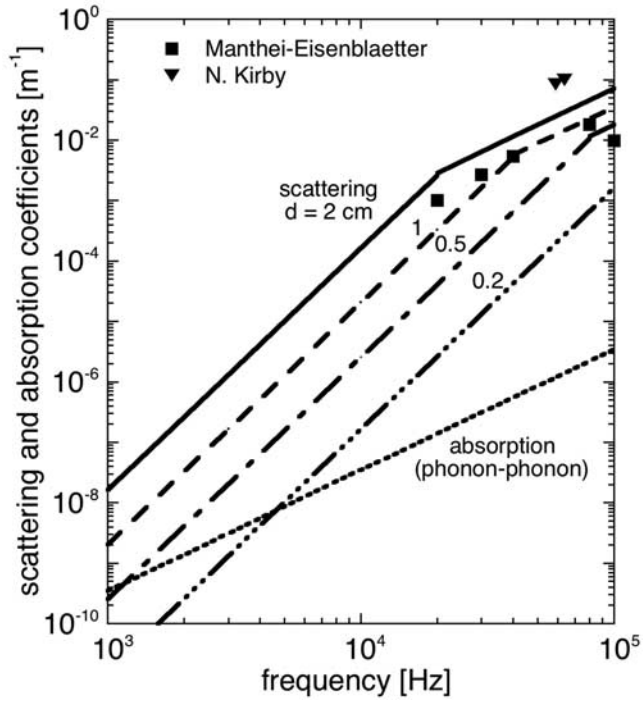


**Figure 7.** Calculated scattering coefficient for grain diameters from 0.2 to 2 cm and absorptivity, (independent of grain diameter), for NaCl. For discussion of data points, see text.

**Table 4.** Summary of Predictions for Antarctic Ice at −51°C and NaCl[a]

| Detector Array | $\lambda_s$ at 10 kHz | $\lambda_s$ at 30 kHz | $\lambda_a$ at 10 kHz | $\lambda_a$ at 30 kHz | $\lambda_{atten}$ at 30 kHz |
|---|---|---|---|---|---|
| Ice ($d$ = 0.2 cm) | 2000 | 25 | 8–12 | 8–12 | ∼7 |
| Ice ($d$ = 0.4 cm) | 250 | 3 | 8–12 | 8–12 | ∼2.3 |
| NaCl ($d$ = 0.75 cm) | 120 | 1.4 | $3 \times 10^4$ | 3300 | ∼1.4 |

[a]In units of km.

which it can be inferred that equation (16) is valid for frequencies ≪100 GHz and that absorptivity is proportional to frequency and independent of temperature.

[25] I used equation 16 to calculate absorptivity of NaCl. The result is shown as the dotted line in Figure 7 labeled absorption (phonon-phonon). This agrees with laboratory data for acoustic absorptivity of NaCl [*Sahasrabudhe and Lambade*, 1998], scaled in $f^2$ from the megahertz to the kilohertz regime. Clearly, at frequencies relevant to electromagnetic cascade detection (∼10 to ∼60 kHz), absorption is negligible compared with scattering.

## 9. Ambient Acoustic Noise in Glacial Ice and Salt Domes

[26] At the highest frequency, ∼30 Hz, the seismic station 275 m deep in ice ∼8 km from South Pole has the lowest noise of all stations in the Global Seismic Network (R. Butler, private communication, 2005). Modeling by *Albert* [1998] has shown that station noise will be far lower still at greater depths, due to refraction of station-generated acoustic waves in the strong density gradient of the firn, which bends most of them back up to the surface.

[27] Glacial ice at the South Pole flows toward the ocean at a surface rate of nearly 10 m $yr^{-1}$, whereas at bedrock the rate is close to zero. Most of the shear occurs near bedrock where the temperature is warm enough for plastic deformation to occur. If the shear is of the stick-slip type, discrete acoustic emissions may occur close to or at bedrock. Laboratory experiments on creep deformation of ice at −10°C show that acoustic emissions are broadly distributed in frequency from ∼0.01 to 1 MHz [*Weiss and Grasso*, 1997]. Microearthquakes that originated within a few meters of the base of the ice beneath Ice Streams B and C in West Antarctica have been studied by *Anandakrishnan and Bentley* [1993]. Noise as a function of frequency and time will be measured in South Pole ice with a small array in 2006 (J. Vandenbroucke et al., SPATS: South Pole acoustic test setup, unpublished technical design report, 2005).

[28] Creep due to slow upthrust of a salt dome is accompanied by acoustic emissions in the frequency band 1 to 100 kH, mostly at boundaries between rock salt and clay or anhydrite [*Spies and Eisenblätter*, 2001]. The frequency of occurrence ranges from ∼10 events $h^{-1}$ for small events to short bursts of as many as 200 events $h^{-1}$ every several months. A detailed discussion of creep of rock salt in domes is given by *Carter et al.* [1993].

## 10. Discussion and Conclusions

[29] As shown in Table 1, both ice and salt have much more favorable Grüneisen parameters than ocean water, which means that the threshold for detection of ultrahigh-energy neutrinos is much lower for detectors in ice or salt than for those in the ocean. In addition, ambient noise in the ocean is continuous and much more intense than in ice or rock salt, except during brief intervals of acoustic emission due to creep or stick slip in ice and salt.

[30] At frequencies relevant to future searches for hydrodynamic waves emitted in ultrahigh-energy neutrino-induced cascades (10–60 kHz), both glacial ice and salt domes look promising. As shown in Table 4, due to the small grain size of South Pole ice (∼0.2 cm in the top 600 m, increasing to ∼0.4 cm at 1500 m) compared with a typical value ∼0.75 cm for NaCl in salt domes), ice scatters less strongly than NaCl, whereas ice, due to its hydrogen-bonded structure, absorbs more strongly than NaCl. The last column gives predicted net attenuation length, $\lambda_{atten}$, at 30 kHz, defined as $1/\lambda_{atten} = 1/\lambda_s + 1/\lambda_a$. In view of the scarcity of experimental data for ice and salt at the relevant frequencies, the values in Table 4 are probably not valid to better than ∼50%.

[31] Laboratory measurements of grain boundary scattering in magnesium, which has a hexagonal crystal structure like ice, and of iron and copper, which have cubic structures like NaCl, agree with theory to within a factor 3 throughout the Rayleigh and stochastic regimes [*Merkulov*, 1957a].

[32] In situ measurements of acoustic absorption in glacial ice were made at frequencies 50–200 Hz [*Brockamp and Kohnen*, 1965; *Bentley and Kohnen*, 1976]. Although they are at frequencies too low to be directly applicable to thermoelastic waves from cascades, the values agree with theory for those frequencies. No in situ measurement of scattering, as distinct from attenuation, has been made in glacial ice. From the few in situ data for glacial ice (Figure 6) and salt (Figure 7), extrapolated to frequencies 10 to 60 kHz, it is clear that South Pole ice has adequately long absorption and scattering lengths to serve as the host medium for an observatory with up to $10^4$ $km^2$ surface × 1 km depth, and that the Morsleben salt mine, of dimensions ∼3 km × ∼4 km × ∼5 km, may also be suitable for a large observatory.

[33] In order to take the next step in evaluating the merits of salt domes and South Pole ice, it is essential to make detailed in situ measurements of scattering, absorption, and ambient acoustic noise as a function of depth and frequency in South Pole ice and as a function of frequency and grain size in salt domes. In particular, searches should be made and measurements carried out for mines with mean grain size less than that at Morsleben. In ice the largest uncertainty is the magnitude of attenuation in the firn. (Recall that the acoustic/radio array would be located at depths ∼5 to ∼1500 m.) In salt domes the largest uncertainty is the magnitude of scattering and absorption in clay, liquid inclusions, and anhydrite layers.

[34] **Acknowledgment.** I thank the National Science Foundation for partial support through the IceCube MRE and two anonymous referees for very helpful comments.

## References


Ahrens, J., et al. (2004), Sensitivity of the IceCube detector to astrophysical sources of high energy muon neutrinos, *Astropart. Phys.*, *20*, 507–532.

Akhieser, A. (1939), On the absorption of sound in solids, *J. Phys. USSR*, *1*, 277–287.

Albert, D. G. (1998), Theoretical modeling of seismic noise propagation in firn at the South Pole, Antarctica, *Geophys. Res. Lett.*, *25*, 4257–4260.

AMANDA Collaboration: Askebjer, P., et al. (1997), Optical properties of deep ice at the South Pole: Absorption, *Appl. Opt.*, *36*, 4168–4180.

Anandakrishnan, S., and C. R. Bentley (1993), Micro-earthquakes beneath Ice Streams B and C, West Antarctica: Observations and implications, *J. Glaciol.*, *39*, 455–462.

Askariyan, G. A. (1957), Hydrodynamic radiation from the tracks of ionizing particles in stable liquids, *Sov. J. At. Energy*, *3*, 921–923.

Askariyan, G. A. (1979), Acoustic detection of high energy particle showers in water, *Nucl. Instrum. Methods*, *164*, 267–278.

Askebjer, P., et al. (1997), UV and optical light transmission properties in deep ice at the South Pole, *Geophys. Res. Lett.*, *24*, 1355–1358.

Bentley, C. R., and H. Kohnen (1976), Seismic refraction measurements of internal friction in Antarctic ice, *J. Geophys. Res.*, *81*, 1519–1526.

Besson, D., S. Böser, R. Nahnhauer, P. B. Price, and J. A. Vandenbroucke (2005), Simulation of a hybrid optical/radio/acoustic extension to IceCube for EeV neutrino detection, *Proc. Int. Cosmic Ray Conf., 29th*, in press.

Brockamp, B., and H. Kohnen (1965), Bei Beitrag zu den seismischen Untersuchungen auf dem groenlandischen Inlandeis, *Polarforschung*, *5*, 2–12.

Carter, N. L., S. T. Horseman, J. E. Russell, and J. Handin (1993), Rheology of rocksalt, *J. Struct. Geol.*, *15*, 1257–1271.

De La Chapelle, S., O. Castelnau, V. Lipenkov, and P. Duval (1998), Dynamic recrystallization and texture development in ice as revealed by the study of deep ice cores in Antarctica and Greenland, *J. Geophys. Res.*, *103*, 5091–5105.

Fisher, F. H., and V. P. Simmons (1977), Sound absorption in sea water, *J. Acoust. Soc. Am.*, *62*, 558–564.

Fletcher, N. H. (1970), *The Chemical Physics of Ice*, Cambridge Univ. Press, New York.

Gold, T., and S. Soter (1970), Apollo 12 seismic signal: Indication of a deep layer of powder, *Science*, *169*, 1071–1075.

Gorham, P., D. Saltzberg, A. Odian, D. Williams, D. Besson, G. Frichter, and S. Tantawi (2002), Measurements of the suitability of large rock salt formations for radio detection of high-energy neutrinos, *Nucl. Instrum. Methods, Sect. A*, *490*, 476–491.

Jackson, M. P. A., B. C. Vendeville, and B. C. Vendeville (1994), Structural dynamics of salt systems, *Annu. Rev. Earth Planet. Sci.*, *22*, 93–117.

Kirby, N. (2004), Attenuation and velocity measurements of ultrasound in rock salt, Senior thesis, Univ. of Tex. at Austin, Austin.

Kor, S. K., and P. K. Mishra (1975), Study of phonon-phonon interaction and electron-lattice interaction in alkali metals, *J. Appl. Phys.*, *46*, 506–509.

Kuroiwa, D. (1964), Internal friction of ice, *Contrib. Inst. Low Temp. Sci. Hokkaido Univ. A*, *18*, 1–62.

Lipenkov, V. Y., N. I. Barkov, P. Duval, and P. Pimienta (1989), Crystalline texture of the 2083 m ice core at Vostok station, Antarctica, *J. Glaciol.*, *35*, 392–398.

Lyamshev, L. M. (1992), Radiation acoustics, *Sov. Phys. Usp.*, *35*, 276–302.

Manthei, G., and J. Eisenblätter (2005), Experience on acoustic wave propagation in rock salt in the frequency range 1–100 kHz and conclusions with respect to the feasibility of a rock salt dome as neutrino detector, paper presented at International ARENA Workshop, held May 17–19, 2005, Detsch. Elektro.-Synchrotron, Zeuthen, Germany.

Merkulov, L. G. (1957a), Investigation of ultrasonic scattering in metals, *Sov. Phys. Tech. Phys.*, *1*, 59–69.

Merkulov, L. G. (1957b), Absorption and diffusive scattering of ultrasonic waves in metals, *Sov. Phys. Tech. Phys.*, *3*, 953–957.

Merkulov, L. G., R. V. Kovalenok, and E. V. Konovodchenko (1970), Orientation dependence of the absorption of ultrasound in alkali halide crystals, *Sov. Phys. Solid State*, *11*, 2241–2248.

Oguro, M., K. Hatano, and S. Kato (1982), Orientation dependence of internal friction in artificial single crystals of ice, *Cold Regions Sci. Technol.*, *6*, 29–35.

Palik, E. D. (1985), Sodium chloride, in *Handbook of Optical Constants of Solids*, edited by E. D. Palik, pp. 775–793, Elsevier, New York.

Paterson, W. S. B. (1994), *Physics of Glaciers*, 3rd ed., Elsevier, New York.

Price, P. B. (1993), Mechanisms of attenuation of acoustic waves in Antarctic ice, *Nucl. Instrum. Methods, Ser. A*, *325*, 346–356.

Price, P. B., O. V. Nagornov, R. Bay, D. Chirkin, Y. He, P. Miocinovic, A. Richards, K. Woschnagg, B. Koci, and V. Zagorodnov (2002), Temperature profile for glacial ice at the South Pole: Implications for life in a nearby subglacial lake, *Proc. Natl. Acad. Sci. U.S.A.*, *99*, 7844–7847.

Sahasrabudhe, G. G., and S. D. Lambade (1998), Temperature dependence of ultrasonic Grüneisen parameter and ultrasonic attenuation in alkali halides, *J. Acoust. Soc. Am.*, *104*, 81–85.

Schiller, P. (1958), Die mechanische Relaxation in reinen Eiseinkristallen, *Z. Phys.*, *154*, 1–15.

Spies, T., and J. Eisenblätter (2001), Acoustic emission investigation of microcrack generation at geological boundaries, *Eng. Geol.*, *61*, 181–188.

Thorsteinsson, T., J. Kipfstuhl, and H. Miller (1997), Texture and fabrics in the GRIP ice core, *J. Geophys. Res.*, *102*, 26,583–26,600.

Weiss, J., and J.-R. Grasso (1997), Acoustic emission in single crystals of ice, *J. Phys. Chem. B*, *101*, 6113–6117.


P. B. Price, Physics Department, University of California, Berkeley, CA 94720, USA. (bprice@berkeley.edu)